RSC Advances

PAPER

View Article Online
View Journal | View Issue

Cite this: *RSC Adv.*, 2024, **14**, 37498

Establishment of a Raman microsphere-based immunochromatographic method for the combined detection of influenza A and B viruses and SARS-CoV-2 antigen on a single T-line†

Aolin Zhu, ‡[a] Binbin Zhao, ‡[a] Jiutong Li,[ab] Xinxia Li,[ac] Qian Shi,[d] Xin Zhang,[d] Dongmei Lu*[e] and Dong Yan*[af]

A simple and rapid method based on Raman microsphere immunochromatography was developed in this study for the simultaneous detection of influenza A and B viruses and SARS-CoV-2 on a single test T-line. Three types of Raman microspheres with different Raman characteristics were used as the signal sources and were labelled with monoclonal antibodies against FluA, FluB and SARS-CoV-2, respectively. A mixture of antibodies containing anti-FluA monoclonal antibody, anti-FluB monoclonal antibody and anti-SARS-CoV-2 was sprayed on the detection line (T), and goat polyclonal antibody to chicken (IgY) encapsulated on the quality control line (C), for qualitative detection of these three viruses by the double antibody sandwich method. The results demonstrated that the LOD values were 0.5 ng mL^{-1} for FluA, 0.25 ng mL^{-1} for FluB, and 0.5 ng mL^{-1} for SARS-CoV-2. The method showed good repeatability for the respiratory viral antigens, with CV values below 15%. Oxymetazoline and commonly used oral medications did not interfere with the test results; the strips did not cross-react with common respiratory virus antigens, demonstrating good specificity. This method does not require any complicated pre-treatment, and all three viruses can be detected simultaneously by titrating one sample, which improves the detection efficiency. The Respiratory Pathogen Multiplex provides a scientific basis for preventing and controlling the spread of respiratory diseases by analyzing data to understand epidemiological trends and the spread of pathogens.

Received 29th July 2024
Accepted 15th October 2024

DOI: 10.1039/d4ra05483k

rsc.li/rsc-advances

1. Introduction

With the gradual metamorphosis of Severe Acute Respiratory Syndrome Coronavirus-2 (SARS-CoV-2) from a pandemic strain to a common epidemic virus, common seasonal respiratory viruses that have been in hiding for the last three years are re-emerging as large-scale epidemics, raising concerns among the public and public health authorities worldwide and gaining increased attention of policymakers.[1] Common seasonal respiratory viruses mainly include influenza viruses, Respiratory Syncytial Virus (RSV), Adenoviruses (ADV) and the common coronavirus. Among them, influenza viruses are classified on the basis of their nucleoprotein (NP) and membrane protein (MP) into four types, namely A, B, C and D.[2] Influenza A viruses can be transmitted from host to host, mainly through genetic recombination, adaptive mutation, and antigenic variations. The lack of sustained human immunity to influenza A viruses has resulted in several pandemics worldwide as this subtype poses the greatest threat to humans. Influenza B viruses tend to spread in small environments,[3] and unlike influenza A viruses, they affect only certain populations, such as children, but are often associated with complications and can be even more harmful to society than influenza A viruses.[4] Coronaviruses can adapt to new hosts across species barriers[5] and can be transmitted from animals to humans,[6] causing a range of predominantly respiratory viral diseases in humans; the symptoms can range from mild fever to severe dyspnea and progress to pneumonia and death. Studies have reported that in some respiratory infections, SARS-CoV-2 is mixed with other respiratory viruses (*e.g.* influenza A, influenza B and RSV, *etc.*), which

[a]*Pharmacy Academy of Xinjiang Medical University, Urumqi, 830054, People's Republic of China. E-mail: 252036104@qq.com*

[b]*Xinjiang Xingyi Bio-Science Co., Ltd, Urumqi, 830011, China*

[c]*Key Laboratory of High Incidence Disease Research in Xinjiang (Xinjiang Medical University), Ministry of Education, Urumqi, 830054, China*

[d]*Department of Clinical Laboratory, Hospital of Xinjiang Production and Construction Corps, No. 232, Qingnian Road, Tianshan District, Urumqi, Xinjiang, China*

[e]*Respiratory and Critical Care Medicine, People's Hospital of Xinjiang Uygur Autonomous Region, Urumqi, Xinjiang 830000, China. E-mail: dongmeilu2009@sina.com*

[f]*Xinjiang Key Laboratory of Biopharmaceuticals and Medical Devices, Urumqi, Xinjiang, China*

† Electronic supplementary information (ESI) available. See DOI: https://doi.org/10.1039/d4ra05483k

‡ These authors contributed equally to this work.

prolongs the duration of the infection[7] and further worsens the patient's health condition, leading to a mental and financial burden. Rapid and accurate identification of respiratory viruses not only aids in the precise clinical use of drugs and timely intervention but also provides a solid basis for epidemiological investigation and devising prevention and control measures as respiratory viruses share similar clinical symptoms and transmission and cross-infection routes.

Methods currently available for the diagnosis of respiratory viruses include virus isolation and culture methods, serological diagnosis, molecular diagnosis and modern immunological diagnosis.[8–11] Traditional virus isolation is the gold diagnostic standard for respiratory viruses,[12] while nucleic acid testing and Enzyme-Linked Immunosorbent Assay (ELISA) are the most widely used techniques for detecting viral antigens and antibodies. These diagnostic methods have absolute advantages in accuracy and authority but are relatively complicated and time-consuming.[13] Nucleic acid testing requires advanced instrumentation and trained personnel and incurs a high cost but does not meet the demand for immediate detection.[14] ELISA experiments involve repeated plate-washing operations, and the steps are laborious.[15] The majority of currently employed diagnostic techniques are unable to satisfy the increasing demand for rapid and large-scale field testing of respiratory viruses.

Lateral flow immunoassay (LFIA) test strips have gained considerable traction as a popular point-of-care testing (POCT) tool largely due to their simplicity, cost-effectiveness, and short detection time.[16] Conventional LFIA utilizes colloidal gold as the labeling agent and is based on color visualization. However, this method is prone to subjectivity as the results are observed through the naked eye, and it presents relatively limited sensitivity and hence is restricted to qualitative or semi-quantitative detection.[17] In recent years, surface-enhanced Raman scattering (SERS) as an optical detection technology has garnered increased interest due to the numerous advantages it offers, including narrow spectral peaks, low optical drift, strong multiplexing ability, high sensitivity, simple operation, fingerprint spectra and the ability to identify a vast number of substances in a single analysis. SERS has found widespread use in protein, bacterial, pathogen and small molecule analyses.[18,19] SERS is capable of providing accurate fingerprints even for complex samples at very low concentrations. Some authors have combined SERS with the flow measurement immunoassay (LFIA) technique. In this approach, functional SERS-encoded nanoparticles (SERS tags) are used as signal reporters instead of colloidal gold, thereby combining high sensitivity and quantitative analysis to significantly enhance the detection limits of immunochromatography.[20] Notably, the detection capability of SERS-based LFIA is contingent on the efficacy of SERS labelling. A number of studies have demonstrated that SERS signals are largely derived from molecules situated in small 'hot spots'. These hot spots can be defined as localized areas where the electric field is significantly enhanced. The interaction of a laser beam with the nanoscale noble-metal structures generates hotspot excitation, which amplifies the Raman signal of the substance undergoing detection.[21] A number of high-performance SERS substrates have been identified by researchers, including gold nanorods (Au NRs), hollow gold nanospheres, and Au@Ag NPs.[22,23] These substrates enable single-molecule detection through SERS technology. Jia *et al.* used Au@Ag core–shell nanoparticles modified with a bilayer of Raman reporter molecules as SERS substrates for the quantitative detection of *Mycoplasma pneumoniae* antibodies with a detection limit of 0.1 ng mL^{-1}.[24] Russo *et al.* used gold and silver nano shells as substrates for Raman signal enhancement in the detection of mycovirus protein A and reported a detection limit of 51.8 ng mL^{-1}.[25]

Recent studies have demonstrated the successful application of SERS-LFA technology to sensitive and quantitative analysis of a diverse range of targets, including viral, inflammatory, and cardiac biomarkers.[26–28] The conjugation of Maria's serially encoded gold nanostars with two disease-specific antibodies could reduce the limit of detection in immunoassays by 15-fold for Zika NS1 and by 7-fold for dengue NS1 for a single line of detection on test strips.[29] Zhang *et al.* developed a new lateral flow analysis (LFA) based on Raman dyes (RDs) encoding core–shell surface-enhanced Raman scattering (SERS) nanolabels, which could rapidly quantify three cardiac biomarkers on a single test (T) line, proving valuable in the early diagnosis of acute myocardial infarction (AMI).[30] The multiplexing capability of a color-coded assay was demonstrated by Di *et al.* based on the concurrent detection of aflatoxin B1 (AFB1) and fumonisins type B (FBs) in wheat and wheat-derived food products on a single line of detection utilizing red and blue gold nanoparticles conjugated with antibodies directed towards the two distinct analytes.[31] Mao *et al.* devised a novel CHA-based SERS-LFA apparatus, which enabled the simultaneous detection of miR-21 and miR-196a-5p on a single line, thereby greatly improving the detection efficiency and facilitating the quantitative detection of both miRNAs.[32]

The technologies used to achieve SERS-LFIA multiplexing have become more sophisticated over time. However, there is no published work on the possibility of detecting three respiratory pathogens simultaneously on a single test line. Accordingly, the objective of this study was to simultaneously detect three respiratory viruses—influenza A, influenza B, and SARS-CoV-2—on a single T-line by SERS-LFA to reduce reagent consumption and cost, shorten the preparation time, and reduce manual operation. The complexity of the assay and the cost of custom Raman instruments can be significantly reduced with a single T-line. Additionally, the multiplicity of a single T-line can be enhanced by utilizing multiple color-coded SERS nanotags. The qualitative test was selected for subsequent ease of use in the clinic. Using the triple test reagent card, only the cutoff value (Yblank + 3SD, Y is the Raman signal value) of each batch of the product can be measured, and a result higher than the cutoff value is considered positive, while a result lower than the cutoff value is considered negative. This allows the direct determination of whether a patient is sick or not. Therefore, this study provides guidance for clinicians to identify patients for

treatment and avoid blind drug use and mixed infections, offering a reference for clinical diagnosis.

2. Experimental methods

2.1. Instrumentation and materials

The CT14RD tabletop high-speed freezing centrifuge was obtained from Shanghai Tianmei Biochemical Instrument and Equipment Engineering Co., Ltd. The BSM-220.4 electronic balance was obtained from Shanghai Zhuojing Electronic Technology Co., Ltd. The T-DOA desktop dotting and spraying machine was obtained from Hangzhou Han Sense Technology Co., Ltd. UV-vis adsorption spectra were collected on a spectrometer (L6S, Shanghai Yidian Scientific Instrument Co., Ltd). Transmission electron microscopy (TEM) images of the SERS nanotags were captured by TEM (JEOL JEM-F200, Japan). The diameter and zeta potential values of the nanoparticles were measured on a ZetaSizer Nano ZS90 (Malvern, UK). The Raman spectra of the SERS nanorods and the detection T-line were obtained on a portable Raman spectrometer (Shanghai Lidong Optoelectronic Technology Co., Ltd). For spectral processing, Flavor software, version 1.3.7-R20210805 which accompanies the BLADE-785B-OEM handheld Raman spectrometer was used. The software allows the direct deduction of background baseline and fluorescence signals from the acquired SERS signals and presents them in real time. The algorithm and logic of this process are provided in the ESI (S1).† The excitation wavelength of the laser was 785 nanometres (nm), with a spot diameter of 100 micrometres (μm). The laser power was 100 milliwatts (mW) for each measurement, with an acquisition time of 250 milliseconds (ms).

Disodium hydrogen phosphate, sodium dihydrogen phosphate, sodium chloride, aminomethane (Tris), Tween 20, Triton X-100, and sodium chloride (Analytically Pure) were purchased from Sinopharm Chemical Reagent Co., Ltd. PVC base plates and sample pads were purchased from Shanghai Gold Standard Biotechnology Co., Ltd. The Fusion 5 sample pads were purchased from Whatman. The water absorbent pads were purchased from Shanghai Jining Biotechnology Co., Ltd. Bovine serum albumin (BSA) was purchased from Genview. Proclin 300 was purchased from Merck Sigma. Casein was purchased from Tokyo Kasei Kogyo Co., Ltd. The influenza A virus antibody (including the tracer antibody 006 and the capture antibody 009) and the influenza B virus capture antibody 012 were purchased from Fipon Biological Co., Ltd. The influenza A virus antigen was purchased from Suzhou Nearshore Protein Technology Co., Ltd. Sheep anti-chicken antibody was purchased from Chongqing Tansheng Technology Co., Ltd. The influenza B virus antigen and respiratory syncytial antigen were purchased from Shenzhen Heavy Chain Biotechnology Co., Ltd. The SARS-CoV-2 antigen was purchased from Xiamen Wanbo Bio-Technology Co., Ltd. The SARS-CoV-2 antibodies (including tracer antibody 415-1 and capture antibody 415-2) were purchased from Guangzhou Wanfu Bio-technology Co., Ltd. The adenovirus antigen was purchased from Sea Peptide Biotechnology (Shanghai) Co., Ltd. The *Mycoplasma pneumoniae* antigen was purchased from Shenzhen Heavy Chain Biotechnology Co., Ltd. The Parainfluenza Virus Antibody was purchased from Suzhou East Antibody Co., Ltd. R-Sphere^{006}, R-Sphere^{013} and R-Sphere^{026} were obtained from Shanghai Simp Diagnostic Biotechnology Co., Ltd. The experimental water was ultra-pure water obtained from a CJ-A06 system (18.2 MΩ cm^{-1}).

2.2. Synthesis of antibody-conjugated SERS nanotags

To prepare antibody-functionalized SERS nanolabels, FluA monoclonal antibody 006, FluB monoclonal antibody 9C3 and SARS-CoV-2 monoclonal antibody 154 were electrostatically adsorbed onto the surface of R-Sphere^{013}, R-Sphere^{006} and R-Sphere^{026}, respectively, to form antibody-coupled SERS nanolabels. Briefly, to 1 mL each of the prepared R-Sphere^{006}, R-Sphere^{013} and R-Sphere^{026} solutions, 7.5 μg of influenza B virus 9C3 tracer antibody, influenza A virus 006 tracer antibody and SARS-CoV-2 415-1 tracer antibody were added, respectively; the samples were mixed well to react for 15 min, and then 10 μL of 10% BSA was added to close the active end of the unreacted antibodies. After final mixing and reaction for 10 min, the samples were centrifuged (4 °C, 8000 rpm) for 10 min, and the supernatant was discarded. To each of the samples, 100 μL of ultra-pure water was added to redissolve the precipitate to obtain the R-Sphere^{006}-mAb^{FluB}, R-Sphere^{013}-mAb^{FluA} and R-Sphere^{026}-mAb$^{SARS\text{-}CoV\text{-}2}$ solutions, which were evenly spread on a 2.5 × 5 cm binding pad and dried for 2 h.

2.3. Preparation of a series of standard antigenic solutions

The PBS solution with 1‰Triton was used as the lysate to prepare specific concentrations of influenza A and B viruses and SARS-CoV-2 antigens. A series of standard solutions were prepared by mixing them to achieve respective concentrations (Table 1).

2.4. Preparation of test strips

Test strips were prepared as described in the literature.[33] The NC membrane (length: 25 mm) was attached to the middle of the PVC backing (length: 80 mm), and a 1 : 1 equimolar mixture of 0.8 mg mL^{-1} sheep anti-chicken antibody IgY and three capture antibodies (0.4 mg per mL FluA 009 capture antibody, 0.4 mg per mL FluB 012 capture antibody and 0.4 mg per mL SARS-CoV-2 172 capture antibody) was applied to the NC membrane at a rate of 0.8 μL cm^{-1}, followed by a two-hour drying period. Two lines were then produced, with one designated as the control (C) line and the other as the T line. The two lines were separated by a distance of 5 mm. The sample pad (length: 17 mm), coupling pad (length: 4 mm) and absorbent pad (length: 18 mm) were attached to both ends of the NC film in sequence, with each pad overlapping the preceding one by

Table 1 Standard solutions of influenza A and B viruses and SARS-CoV-2 antigens

Sample number	1	2	3	4	5	6	7	8
FluA (ng mL^{-1})	0	0.25	0.50	2.00	5.00	10.00	25.00	50.00
FluB (ng mL^{-1})	0	0.25	0.50	2.00	5.00	10.00	25.00	50.00
SARS-CoV-2 (ng mL^{-1})	0	0.25	0.50	2.00	5.00	10.00	25.00	50.00

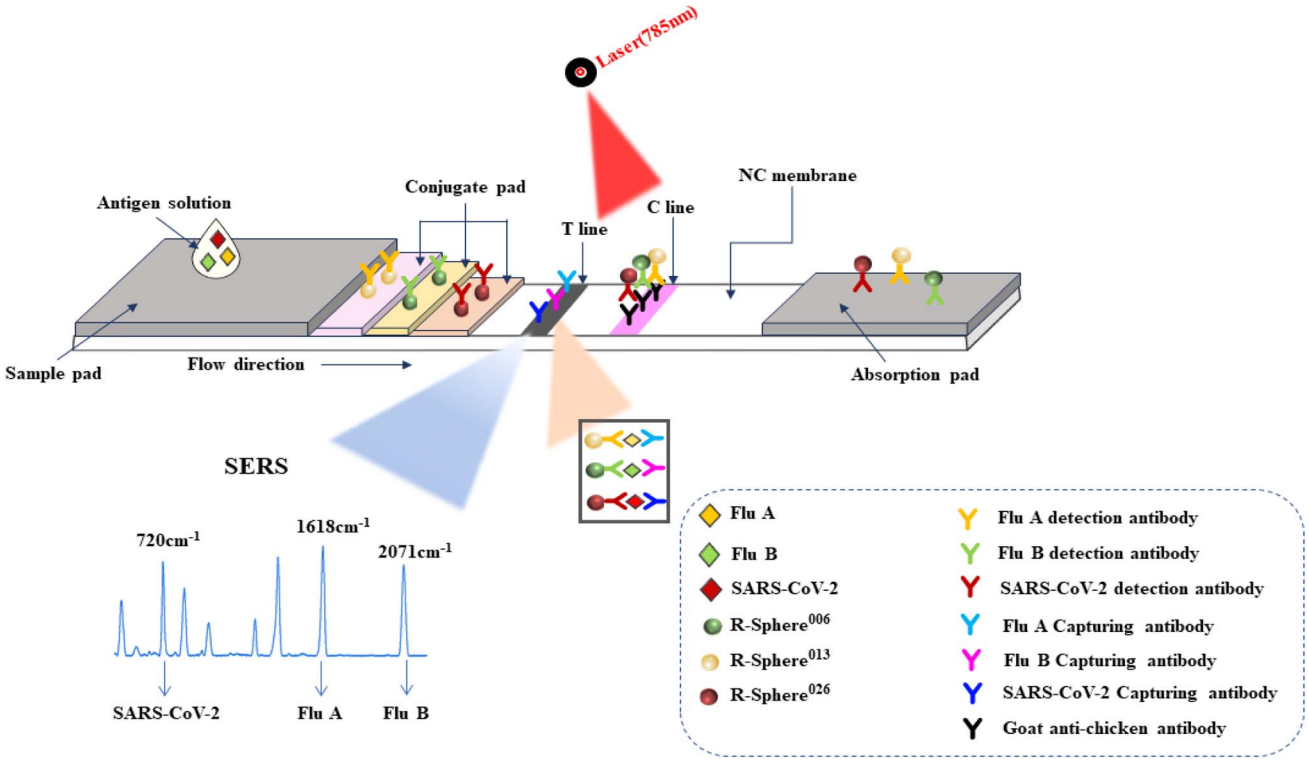

Fig. 1 Schematic overview of the assay for the simultaneous detection of influenza viruses A and B and SARS-CoV-2.

1.0 mm. Subsequently, using a strip cutter, the pads were cut to a width of 3.4 mm and sealed with a desiccant for storage.

3. Results and discussion

3.1. Principle of the immunoassay

Fig. 1 illustrates the basic principles of Raman microsphere-based immunochromatography for the simultaneous identification of influenza A, B virus and SARS-CoV-2 antigens. A mixture of the capture antibodies and the structural proteins of the three pathogens, namely influenza A and B viruses and SARS-CoV-2, is immobilized on the T-line of a nitrocellulose membrane, and the tracer antibodies against the structural proteins of the three pathogens are loaded on the surfaces of the Raman microspheres with their respective characteristic spectra, namely R-Sphere^{013}, R-Sphere^{006} and R-Sphere^{026}, which are mixed and dried on the binding pads. The antigen solution is added dropwise to the sample pad. The sample is chromatographed forward, and the antibodies on the Raman microspheres are re-dissolved. If the sample is positive for one or more viruses in this pathogen group, a specific antigen–antibody reaction takes place at the T-line during chromatography, resulting in the formation of a three-sandwich complex containing the pathogen, which appears grey-black with a certain intensity. The other Raman microsphere antibodies follow the antigen solution and move towards the absorbent pad and are captured by the C-line. If the sample is negative for this group of pathogens, the T-line will not reveal a specific antigen–antibody reaction and will not be stained and will be captured by the C-line as the antigen solution will move towards the absorbent pad. To ensure the validity of the reagent strip, the C-line will show color regardless of whether the result is positive or not. The test strips can be detected for Raman signals at the T-line with a handheld Raman spectrometer, and the spectrograms are analyzed to determine the presence or absence of each pathogen based on the intensity and shifts of the Raman signals at 1618, 2071 and 720 cm^{-1}.

3.2. Nanomaterial characterization

This study involved a typical SERS-based LFIA; silver-shelled nano microspheres with a plasma gold core and molecularly labelled with the Raman reporter (SERS tags) that could be coupled to antibodies and bind to specific target proteins were employed on the T-line. The TEM images (Fig. 2A–C) demonstrated that the R-Sphere^{013}, R-Sphere^{006} and R-Sphere^{026} particles exhibited a spherical morphology with uniform particle size and monodisperse distribution. The dark central region observed in the images represents the gold nanocore, while the outer layer is the light silver shell, which demonstrates the successful synthesis of the nano microspheres. To ascertain the configuration of the synthesized nano microspheres, we conducted an elemental mapping analysis of the individual core–shell nano microspheres. The distributions of Au and Ag are indicated in red and green (Fig. 2II and III), respectively, and the energy spectroscopy (EDS) analysis substantiated the simultaneous presence of Au and Ag in the R-Spheres (Fig. 2IV), indicating that the weight proportions of Au and Ag were

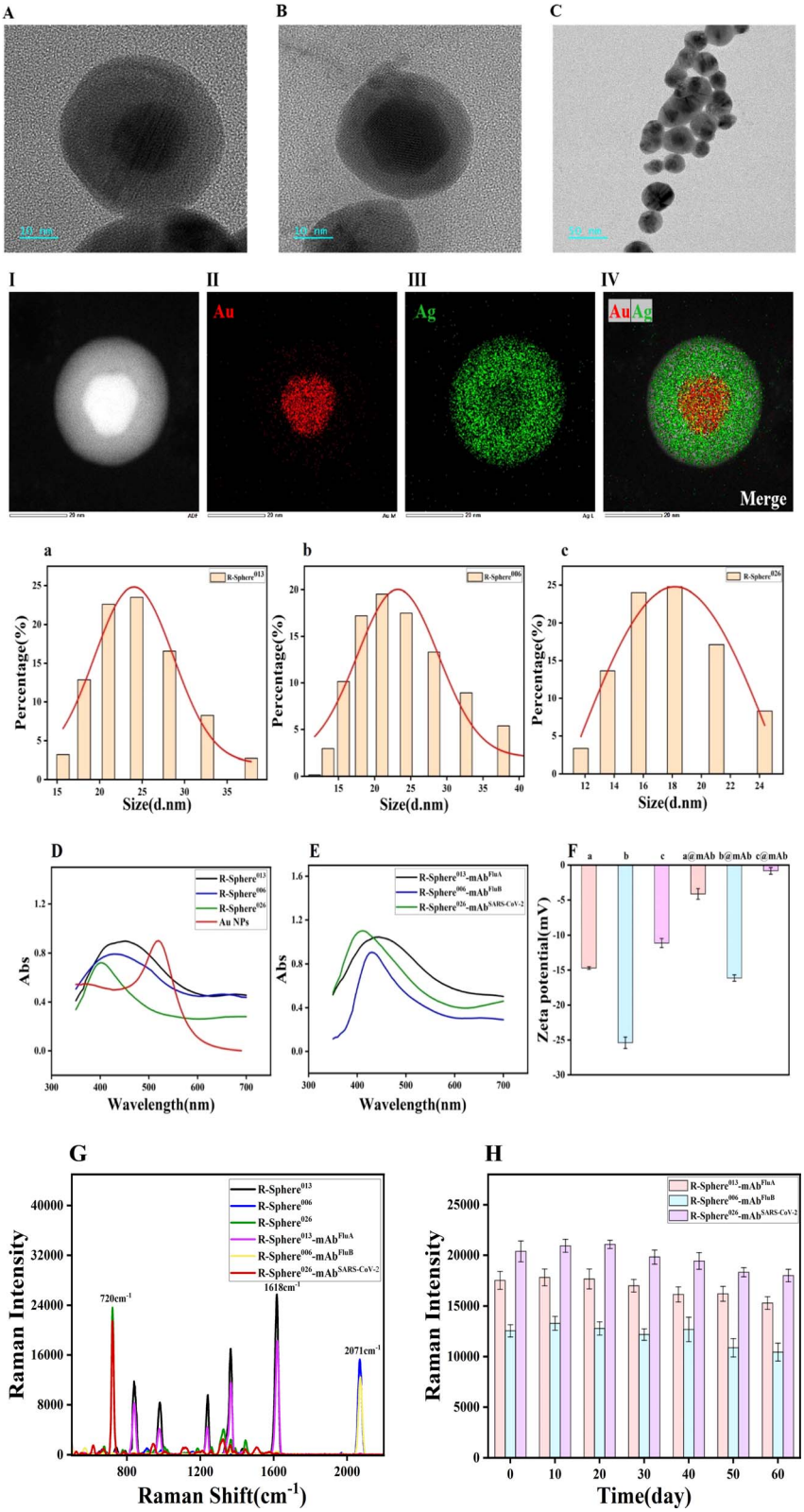

Fig. 2 TEM of (A) R-Sphere^{013}, (B) R-Sphere^{006} and (C) R-Sphere^{026}; (I–IV) elemental mapping images of the R-Spheres; (a–c) size distribution; (D) UV-vis images of Au@Ag NPs, R-Sphere^{013}, R-Sphere^{006} and R-Sphere^{026}; (E) UV-vis plots of antibody-coupled nanomicrospheres; (F) zeta potentials of the as-obtained samples during different stages; (G) SERS spectra of the nanomicrospheres and antibody-coupled nanomicrospheres under the same test conditions; (H) relationship between the Raman intensity of nanomicrospheres coupled with antibodies at 1618 cm^{-1}, 2071 cm^{-1} and 720 cm^{-1} with and storage time. Error bars indicate the standard deviations measured from three separate experiments.

16.79% and 83.21%, respectively. Moreover, the diameter of R-Sphere^{013} obtained by nanoparticle size analysis was about 24.51 ± 5.23 nm, while that of R-Sphere^{006} was approximately 21.28 ± 5.23 nm, and that of R-Sphere^{026} was approximately 18.16 ± 3.86 nm (Fig. 2a–c).

The UV-visible absorption spectra of the Au NPs, R-Sphere013, R-Sphere006 and R-Sphere026 in the wavelength range of 350–750 nm are presented in Fig. 2D. The maximum absorption peak of Au was at 520 nm. The maximum absorption peaks of R-Sphere^{013}, R-Sphere^{006} and R-Sphere^{026} marked in black, blue and green were observed at the wavelengths of 450 nm, 430 nm and 410 nm, respectively. These corresponded with the characteristic absorption peak of Ag when Ag was encapsulated on the surface of the Au NPs, thus indicating the successful synthesis of the Au@Ag core–shell structure. The UV-visible absorption spectra of the SERS nanotags coupled with the respective antibodies exhibited no change in wavelength, indicating that the labelled antibodies did not affect the Raman microspheres (Fig. 2E). Furthermore, the successful coupling of the antibodies with the SERS nanotags was also indicated by the zeta potential (Fig. 2F). The values were −14.7 ± 5.5 for R-Sphere^{013}, −25.2 ± 6.2 for R-Sphere^{006} and −11.1 ± 5.3 for R-Sphere^{026}. Notably, the zeta potential values changed to −4.1 ± 3.2 for R-Sphere^{013}@mAb^{FluA}, −16.1 ± 5.6 for R-Sphere^{006}@mAb^{FluB}, −0.8 ± 6.9 for R-Sphere^{026}@mAb$^{SARS\text{-}CoV\text{-}2}$ which are higher than those of the unmodified microspheres, indicating electrostatic adsorption of the antibodies on the nanomicrospheres. This change in zeta potential proved that the antibody had been successfully modified on these nanomicrospheres.

The Raman signal intensity was elevated as a consequence of the intensified electric field in the gap resulting from the excitation of the gold nuclei by light interaction.[34] The Raman shifts observed for R-Sphere^{026}, R-Sphere^{013} and R-Sphere^{006} were at 720 cm^{-1}, 1618 cm^{-1} and 2071 cm^{-1}, respectively. Fig. 3G illustrates that the Raman peaks of R-Sphere^{013}, R-Sphere^{006} and R-Sphere^{026} did not interfere with each other. Despite the reduction in the Raman signal, the shifts remained unaltered after antibody coupling. This indicates that the antibody modification exerted a negligible effect on the Raman intensities of the SERS nanotags. This finding establishes the feasibility of simultaneous detection of the three viral antigens. In

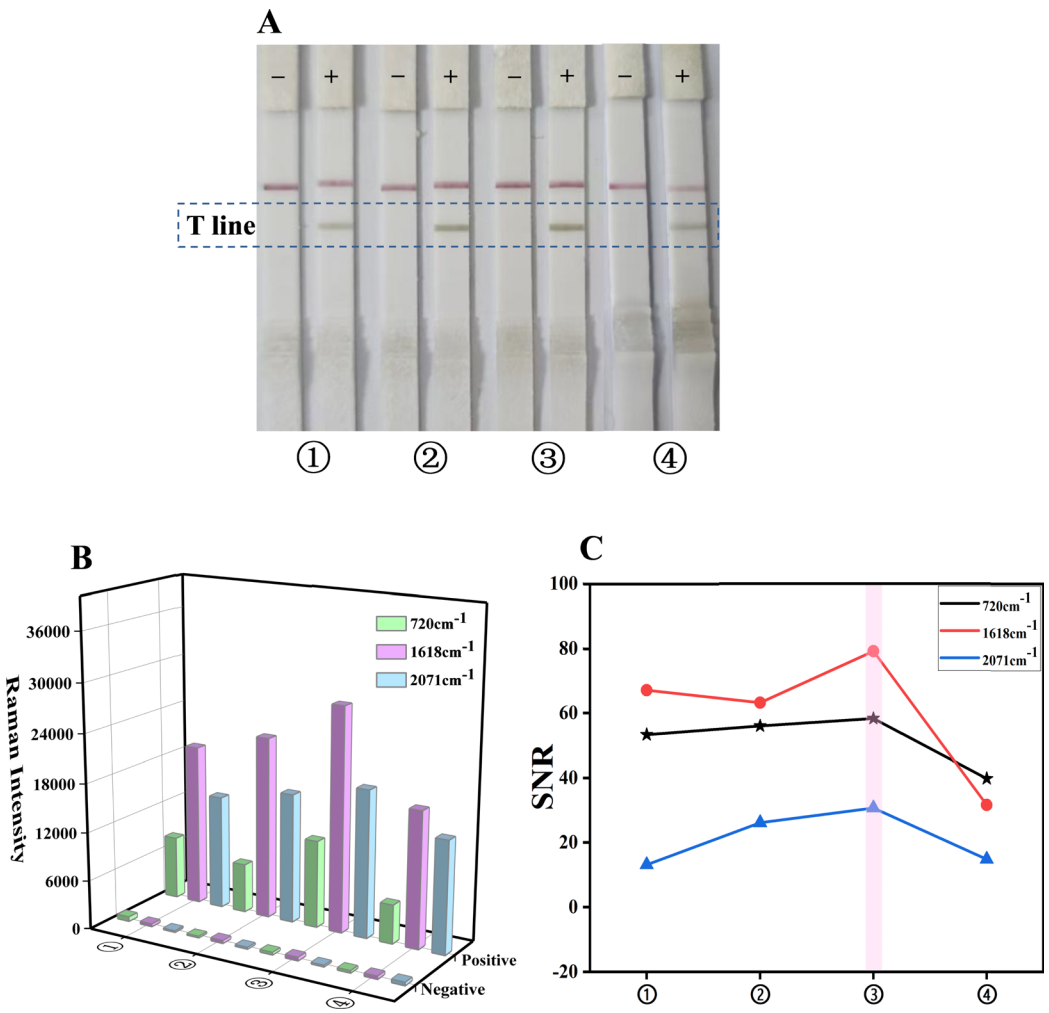

Fig. 3 Optimization of the sample pad treatment solution: (A) photo of the test strips; (B) SERS signals at 720, 1618 and 2071 cm^{-1} of the corresponding T-lines; (C) signal-to-noise ratio.

addition, the Raman microspheres were stored at 4 °C after antibody coupling, and their Raman intensities decreased to some extent with the extension of storage time. After 60 days of storage, their Raman intensities were over 70% of the Raman intensities of the freshly prepared antibody-coupled nanomicrospheres (Fig. 3H), indicating that the SERS nanomicrospheres have good stability after antibody coupling.

3.3. Optimization of the combined influenza A, B virus and SARS-CoV-2 detection system

3.3.1. Screening of the sample pad treatment solution. In this study, the sample pad treatment solution was optimized and four treatment solutions were selected, including ①: 0.1% Casein + 0.6% Tris + 0.5% Tween; ②: 0.1% Casein + 0.6% Tris + 1% BSA; ③: 0.1% Casein + 0.6% Tris + 0.5% Tween + 1% BSA + 0.1% Proclin 300 and ④: Fusion 5 (a single material glass fiber) treated with S17, sucrose and NaCl. After transferring the analytes from the immunoassay into the sample pad, the darkest and most uniformly colored bands with the widest T-line widths were selected as the SERS-LFA bands. Fig. 3A depicts the images of test strips chromatographed with negative and 50 ng mL^{-1} mixed sample solutions of FluA, FluB and SARS-CoV-2. The T-line colors were visible, and the negative strips at numbers ①, ②, ③ and ④ did not show a T-line. Furthermore, the color of the positive T-lines became deeper when 1% BSA was included in the treatment solution. The color of both control line C and test line T was significantly deeper when both 0.5% Tween and 1% BSA were present. Treatment solution ④ was incompletely released from the sample pad during chromatography, resulting in weaker C and T line colors than those of the first three groups. Fig. 3B illustrates the SERS signal intensities at 720, 1618 and 2071 cm^{-1} on the T-line for each test strip depicted in Fig. 3A. The positive SERS signal intensities correlate with the color of the bands on the T-line of the test strips. By analyzing the SNR values detected for the different treatment solutions, it was determined that the optimal detection effect was achieved when the treatment solution contained both 0.5% Tween and 1% BSA (Fig. 3C). Consequently, the sample pad treatment solution no. ③ was selected for subsequent experiments.

3.3.2. Determination of optimal capture antibody concentrations. Next, the concentration of the capturing antibodies on the T-line was optimized, and the Raman signal increased with the concentration of capturing antibodies on the T-line. Four concentrations of the detecting antibody (0.4, 0.8, 1.0 and 1.2 mg mL^{-1}) were tested on the T-line for influenza A (Fig. 4A and B) using 25 ng mL^{-1} of the influenza A antigen; the negative T-lines were consistent with the expectations, and the color of the bands of the T-lines of the positive test strips remained relatively stable. The SERS signal of the T-lines indicated that both the negative and positive Raman signals increased in proportion to the concentration. The SNR value was determined to be the highest when 1.0 mg mL^{-1} of influenza A antibody was applied to the T-line. Therefore, 1.0 mg mL^{-1} was selected as the T-line capture concentration of the influenza A antibody in this study. Similarly, test strips with different capture antibody concentrations were subjected to chromatographic analysis using 50 ng mL^{-1} of the influenza B antigen (Fig. 4C and D), and the SNR values were subsequently calculated. It was observed that the SNR values remained equivalent at T-line concentrations of 1.0 mg mL^{-1} and 1.2 mg mL^{-1}. Consequently, the optimal FluB capture antibody concentration of 1.0 mg mL^{-1} was selected based on economic considerations. Similarly, the T-line capture antibody concentration of the novel crown antigen was evaluated using a concentration of 50 ng mL^{-1} of the novel crown antigen, and 1.0 mg mL^{-1} was identified as the optimal capture antibody concentration for the novel crown antigen based on the SNR values (Fig. 4E and F).

3.4. Performance of the triple test strips

3.4.1. Sensitivity testing. The sensitivity of the SERS-LFA test strips was evaluated by testing antigen solutions containing the FluA, FluB and the SARS-CoV-2 antigens at varying concentrations. The limit of detection (LOD) of the test strip in this experimental procedure was defined as the lowest concentration of FluA, FluB and SARS-CoV-2 that resulted in a total Raman intensity value exceeding the cutoff value. The cutoff value was calculated as *Y*blank + 3SD, where *Y*blank is the average SERS signal of the blank control and 3SD is three times the standard deviation of the blank control.[35] Fig. 5A illustrates the images of test strips of 10 blank controls. The negative T lines did not diverge from the norm, and the T line Raman signals were detected using a portable Raman spectrometer. The peaks marked by red hue in figure a correspond to the negative Raman signatures of SARS-CoV-2, FluA and FluB. The cutoff value for SARS-CoV-2 was determined to be 569, while the cutoff values for FluA and FluB were 1810 and 706, respectively.

Subsequently, 100 μL of FluA, FluB and SARS-CoV-2 solutions at varying concentrations (0, 0.25, 0.5, 2, 5, 10, 25 and 50 ng mL^{-1}) were added to the sample pad. As the concentration of the FluA, FluB and SARS-CoV-2 antigens on the sample pad increased, the color of the test line also became darker. The visual limit of detection (vLOD) for qualitative evaluation was defined as the concentration of FluA, FluB and SARS-CoV-2 corresponding to the lightest color of the test line discernible to the naked eye. As illustrated in Fig. 5B–D, the images of the test strips with varying concentrations of FluA, FluB and SARS-CoV-2 antigen solutions were captured by loading 2, 5 and 5 ng mL^{-1} for the detection lines of FluA, FluB and SARS-CoV-2, respectively. It was observed that as the antigen concentration increased, the corresponding Raman signals of the detection line also increased (Fig. 5b–d). The Raman intensity value of FluA exceeded 1810 when the concentration was 0.5 ng mL^{-1}, 569 when the concentration of SARS-CoV-2 was 0.5 ng mL^{-1}, and 706 when the concentration of FluB was 0.25 ng mL^{-1}. These results indicate that the respective LODs for FluA, FluB and SARS-CoV-2 were 0.5 ng mL^{-1}, 0.25 ng mL^{-1} and 0.5 ng mL^{-1}, respectively. Therefore, the sensitivity of the portable Raman spectrometer was approximately four times, twenty times and ten times higher than that of naked-eye visualization.

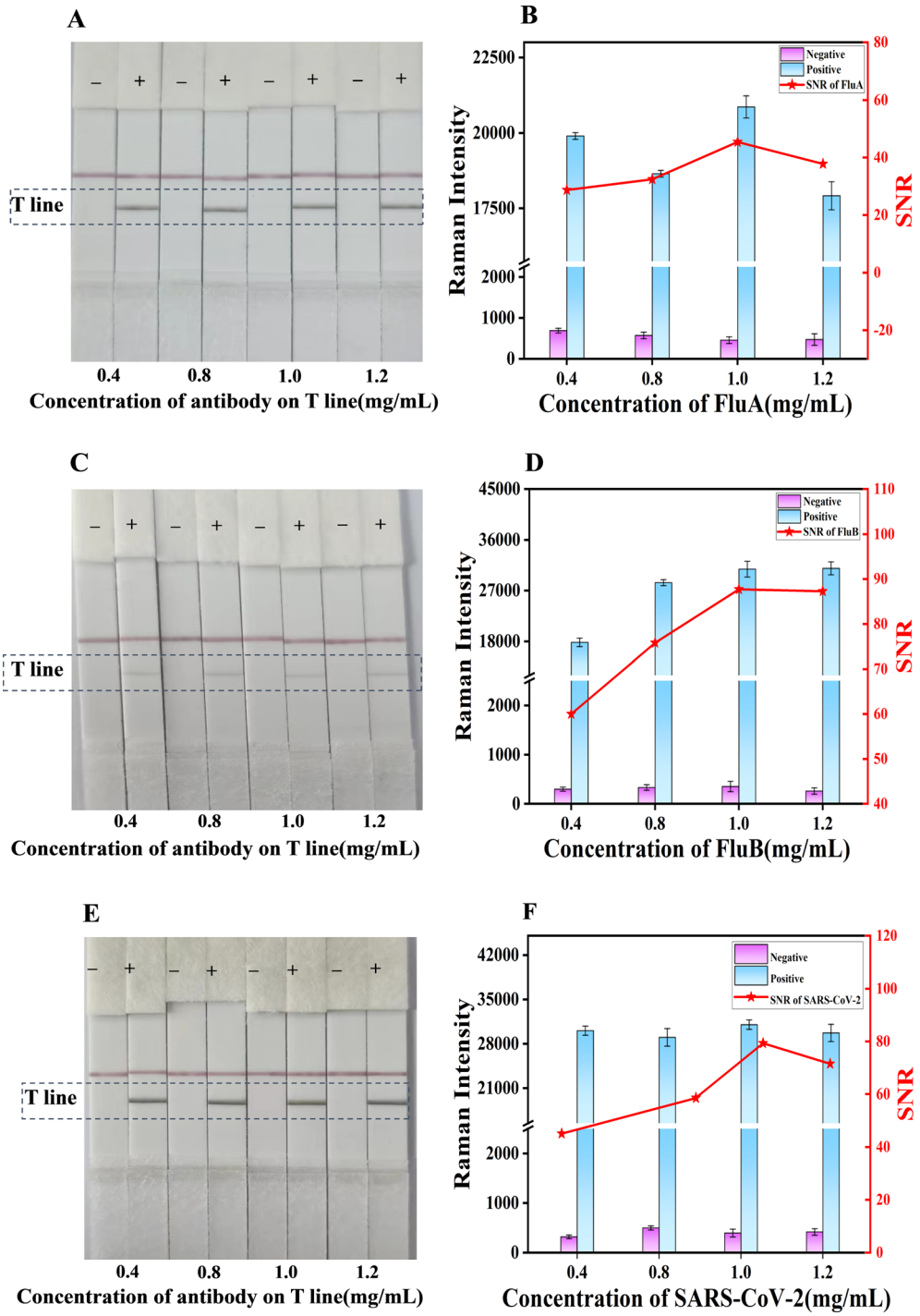

Fig. 4 Optimization of the capture antibody concentrations: (A and B) FluA, (C and D) FluB, and (E and F) SARS-CoV-2.

The established triple detection immunochromatographic system was used for the sensitive detection of mixed solutions of two viruses (influenza A and B/influenza B and SARS-CoV-2/influenza A and SARS-CoV-2) and all three viruses concurrently. This allows for a comparison between the absence of a virus and the identification of a particular virus, in accordance with the previously calculated cutoff values. Fig. 5E illustrates the images of the test strips containing varying concentrations of FluA and FluB antigens combined. The T-line SERS signal (Fig. 5e) indicated an LOD of 0.25 ng mL^{-1} for FluA and 0.25 ng mL^{-1} for FluB. Fig. 5F illustrates the images of the test strips with varying concentrations of FluB and SARS-CoV-2 antigens combined. The T-line SERS signal (Fig. 5f) revealed an LOD of 0.25 ng mL^{-1} for FluB and 0.5 ng mL^{-1} for SARS-CoV-2. Fig. 5G illustrates the images of the test strips with varying concentrations of FluA and SARS-CoV-2 antigens combined. The T-line

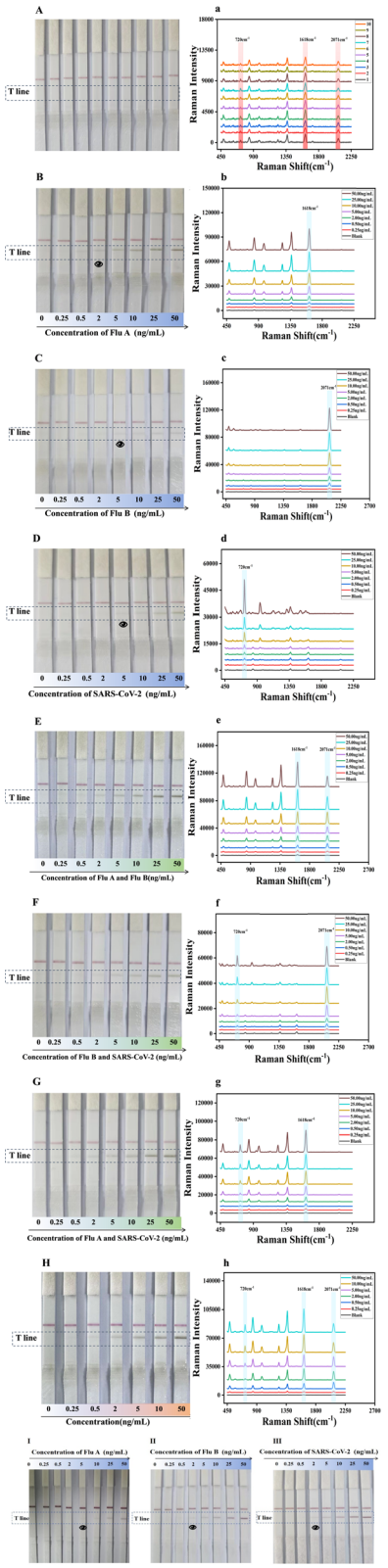

Fig. 5 Results of the sensitivity test of the triple test immunochromatographic test strips: (A) 10 blank controls; (a) corresponding negative Raman signals; (B–D) pictures of test strips with different concentrations of FluA, FluB and SARS-CoV-2 antigen solutions; (b–d) the SERS signal plots corresponding to the different viral antigen concentrations are shown in blue; (E and e) mixture of FluA and B; (F and f) mixture of FluB and SARS-CoV-2; (G and g) mixture of FluA and SARS-CoV-2; (H and h) mixture of all three antigens FluA, FluB and SARS-CoV-2; (I–III) photo of colloidal gold test strips used to detect FluA, FluB and SARS-CoV-2.

SERS signal (Fig. 5g) indicated an LOD of 0.25 ng mL^{-1} for FluA and 0.5 ng mL^{-1} for SARS-CoV-2. When the three samples were mixed, the colour of the T-line turned darker as the concentration increased (Fig. 5H), and the SERS signal was also positively proportional to the concentration (Fig. 5h), yielding an LOD of 0.5 ng mL^{-1} for FluA (1618 cm^{-1}), 0.25 ng mL^{-1} for FluB (2071 cm^{-1}), and 0.5 ng mL^{-1} for SARS-CoV-2 (720 cm^{-1}). These results also match well with the results shown in Fig. S2a–h (ESI).† The LOD values obtained for the mixture of the three viral samples are identical to the LOD results obtained with the individual viruses, indicating that the number of viral sample types present in the solution did not affect the qualitative detection of FluA, FluB, and SARS-CoV-2 on a single T-line. Accordingly, the simultaneous detection of the three viruses on a single T-line is approximately three times more rapid than SERS LFA on three T-lines, which is conducive to rapid detection.

Influenza A, influenza B and SARS-CoV-2 were detected by colloidal gold immunochromatography, as shown in Fig. 5I–III, with visual detection limits of 5.00 ng mL^{-1} for influenza A and 2.00 ng mL^{-1} for influenza B and SARS-CoV-2. Compared with colloidal gold chromatography, the Raman immunochromatographic technique for triple testing established in this experiment presents increased sensitivity to influenza A, influenza B and SARS-CoV-2 by 10, 8 and 8 times, respectively. This indicates that the triple test strips prepared in this work have high sensitivity.

3.4.2. Drug interference experiment. 10 μL nasal spray (oxymetazoline), 10 μL amoxicillin (62.5 mg mL^{-1}), 10 μL loratadine (5 mg mL^{-1}) and 10 μL cefradine (125 mg mL^{-1}) were added to 100 μL of the blank solution. After the addition of these drugs, the T-line showed no visual colors (Fig. 6A). The SERS signals at the T-line were measured with a portable Raman spectrometer, and the Raman signals for the SARS-CoV-2 (720 cm^{-1}), FluA (1618 cm^{-1}) and FluB (2071 cm^{-1}) were below the lowest detection limit. The one-way ANOVA test was employed to analyze the data pertaining to SARS-CoV-2 (Fig. 6a), FluA (Fig. 6b) and FluB (Fig. 6c), respectively. The negative control group and the group with the added drugs were analyzed with respect to the blank, and P values > 0.05 were obtained, which means that there was no significant difference after the addition of the drugs, suggesting that these drugs do not interfere with the triple test strips.

3.4.3. Crossover experiment. To the prepared triple-test immunochromatographic strips, 500 ng mL^{-1} solutions of other common respiratory viral antigens (Respiratory Syncytial Virus, Adenovirus and *Mycoplasma pneumoniae* antigens) were added to validate the specificity of this assay in the presence of non-target test antigens. In addition, to further validate the specificity of this reagent strip, the Raman microspheres were labelled with non-target detection antibodies, including *Mycoplasma pneumoniae* antibodies on R-Sphere^{013}, Parainfluenza

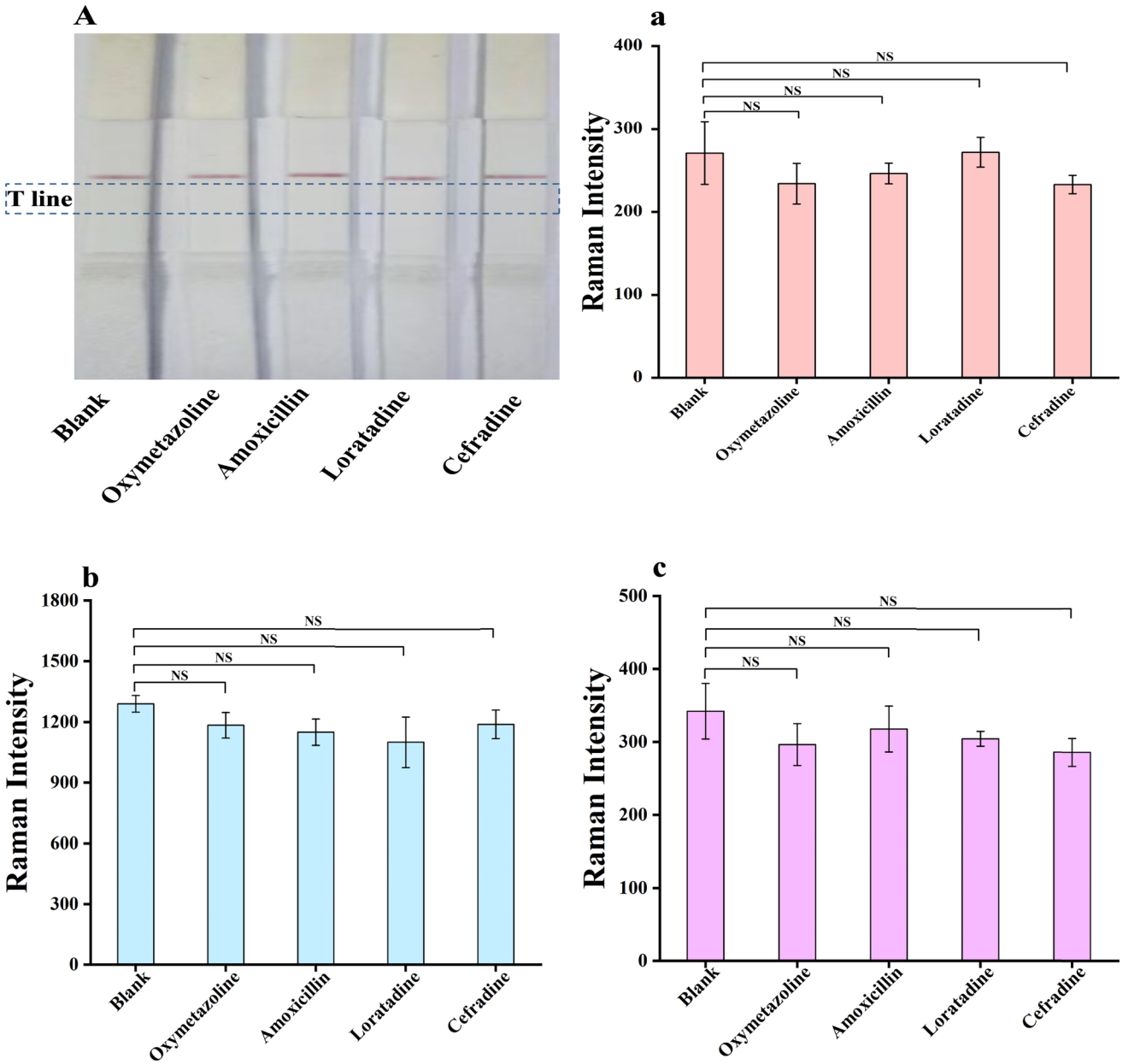

Fig. 6 The drug interference test: (A) picture of the test strips; (a–c) data analysis charts.

Virus Antibodies on R-Sphere^{006} and Respiratory Syncytial Virus antibodies on R-Sphere^{026} and chromatographed with a mixture of FluA, FluB and SARS-CoV-2 antigens. The antibodies and antigens could bind specifically to the target and the T-line appeared as a distinct black line (Fig. 7A). When non-target antigens and non-target antibodies were used, no color appeared in the T-line visualization. However, regardless of crossover, when chromatography was performed with individual FluA, FluB and SARS-CoV-2 antigens, the Raman signals corresponding to FluA, FluB and ARS-CoV-2 appeared very strong. The corresponding T-line Raman signal values obtained with the non-target antigens RSV-Ag, ADV-Ag and MP-Ag and the non-target antibodies MP-Ab, PIV-Ab and RSV-Ab were all below the determined lowest detection limits of the system. Fig. 7a–c present plots of the data analyzed after chromatography of the target antigens, non-target antigens and the non-target antibodies at 720 cm^{-1} for SARS-CoV-2, 1618 cm^{-1} for FluA and 2071 cm^{-1} for FluB. One-way ANOVA of negative and FluA antigens, negative and FluB antigens, and negative and SARS-CoV-2 antigens yielded P values < 0.05, indicating that the chromatography results with specific target antigens were statistically significant. A pairwise analysis between negative and non-target antigens, as well as non-target antibodies, yielded P values > 0.05, which is considered not significant. The above results indicate the excellent specificity of the triple test strips prepared in this work.

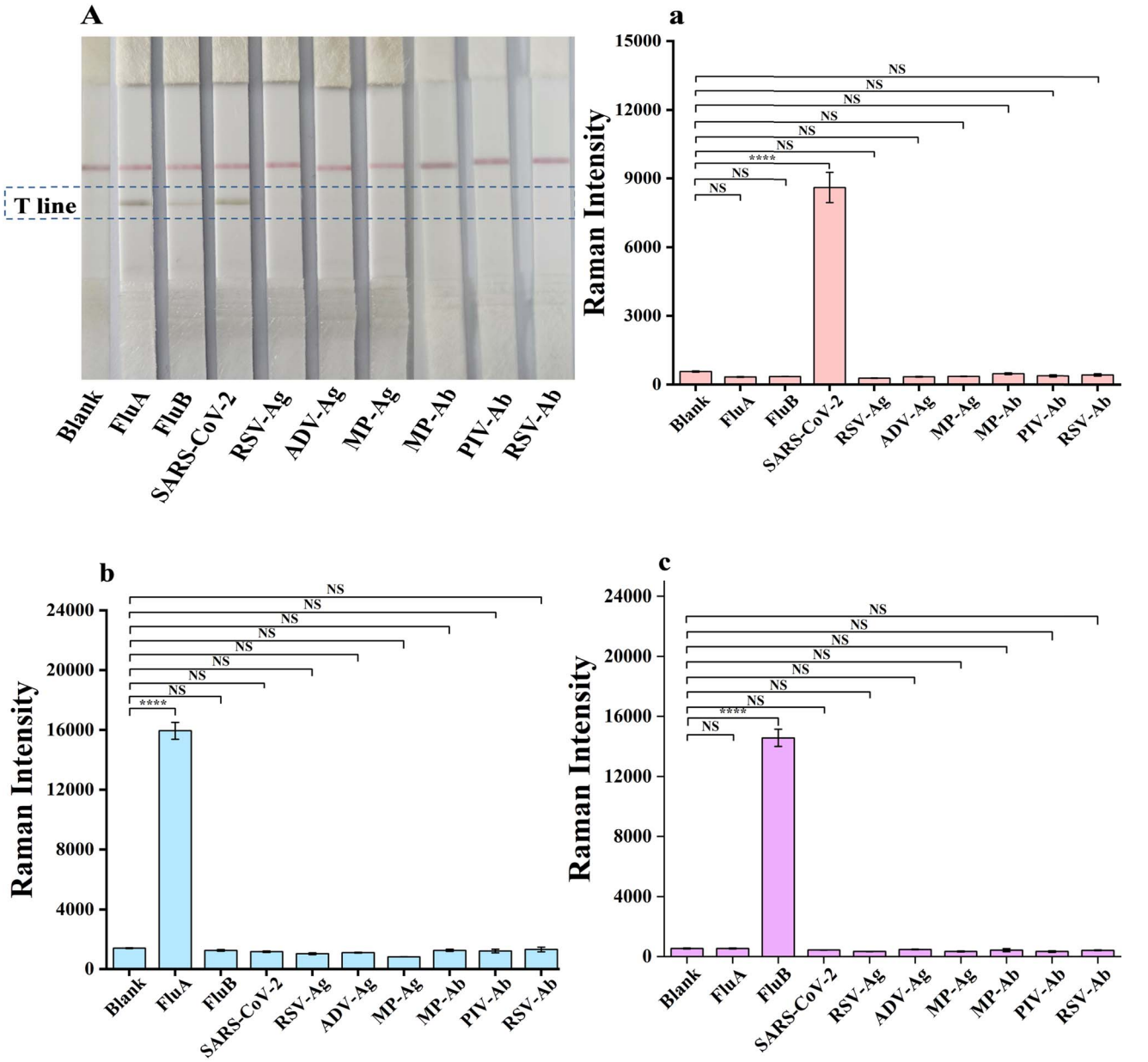

Fig. 7 Results of the crossover studies: (A) photo of the test strips; (a) SARS-CoV-2 signal data analysis; (b) FluA signal data analysis; (c) FluB signal data analysis.

3.4.4. Repeatability experiments. The low-concentration (0.50 ng mL^{-1} for influenza A, 0.25 ng mL^{-1} for influenza B and 0.50 ng mL^{-1} for SARS-CoV-2), medium-concentration (the final concentration of the three viral antigens was 10 ng mL^{-1}) and high-concentration (the final concentration of the three viral antigens was 25 ng mL^{-1}) test strips were taken from the influenza A and B virus and SARS-CoV-2 triple test mixtures. Five test strips of each of the above combinations were chromatographed, and the means and standard deviations were calculated to derive the CV values. Fig. 8A–C illustrate the photographs of the test strips at varying concentrations of the three antigens. The images demonstrate consistent coloration across the T-line bands. The T-line SERS signals were recorded independently in order to facilitate the acquisition of Raman signals for each virus. Fig. 8a depicts the SERS repeatability plots for low, medium and high influenza A concentrations. The coefficient of variation was determined to be 6.39% for low concentrations of influenza A, 7.79% for medium concentrations and 8.42% for high concentrations. Fig. 8b illustrates the SERS reproducibility plots for low, medium, and high concentrations of the influenza B antigen. The coefficient of variation (CV) was calculated to be 11.06% for the low concentration of influenza B, 7.83% for the medium concentration, and 5.51% for the high concentration. Fig. 8c illustrates the SERS

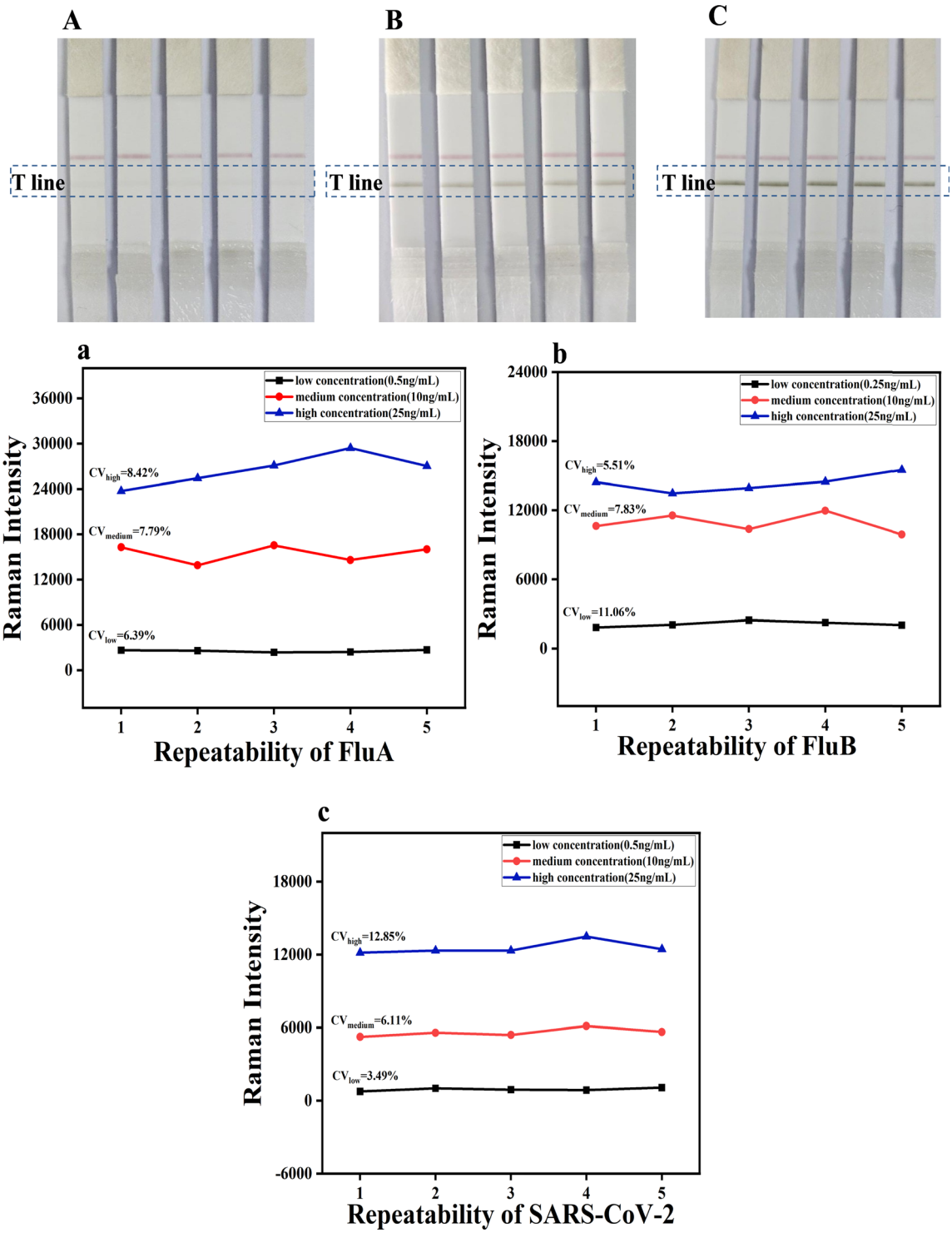

Fig. 8 Results of the repeatability experiments: pictures of the test strips of triple-mixed samples at (A) low concentrations, (B) medium concentrations and (C) high concentrations; SERS repeatability signal maps for (a) influenza A, (b) influenza B and (c) SARS-CoV-2.

reproducibility plots for low, medium, and high concentrations of the SARS-CoV-2 antigen, with a calculated CV of 12.85% for the low concentration, 6.11% for the medium concentration, and 3.49% for the high concentration. The results demonstrated that all CVs were below 15%, indicating good reproducibility of the prepared triple test strips.

4. Conclusion

Based on Raman microsphere immunochromatography, we developed a platform for the rapid, qualitative and simultaneous detection of influenza A, influenza B virus and SARS-CoV-2 on a single T-line. Three kinds of Raman nanoparticles (RNPs)

with different characteristic Raman spectral peak shifts were used to label the three respiratory viruses for simultaneous detection, and the T-line was scanned using a portable Raman spectrometer. The LOD values obtained were 0.5 ng mL^{-1} for influenza A, 0.25 ng mL^{-1} for influenza B, and 0.5 ng mL^{-1} for SARS-CoV-2, which were 10, 8, and 8 times more sensitive than colloidal gold immunochromatography, respectively. In comparison with three T-line SERS LFA, the quantity and cost associated with the requisite reagents are reduced, the preparation time is shorter, and the experimental operation is streamlined, taking only 15 minutes from the start of the test to reading the results, which is conducive to rapid screening of pathogens with similar clinical symptoms. This assay can provide preliminary test results at a reduced cost. In conclusion, Raman microsphere-based immunochromatographic test strips demonstrate a promising future in the detection of respiratory pathogens.

Data availability

Data will be made available on request.

Authorship contributions

Aolin Zhu: original draft, writing – review & editing, methodology, investigation, data curation. Binbin Zhao: original draft, writing – review & editing methodology, investigation, data curation. Jiutong Li: writing – review & editing, supervision, resources, project administration, funding acquisition. Xinxia Li: writing – review & editing, supervision, resources, project administration, funding acquisition. Qian Shi: writing – review & editing, supervision, resources. Xin Zhang: writing – review & editing, supervision, resources. Dongmei Lu: writing – review & editing, supervision, resources, project administration. Dong Yan: writing – review & editing, supervision, resources, project administration, funding acquisition.

Conflicts of interest

There are no conflicts of interest to declare.

Acknowledgements

This research has been funded by the Tianshan Talent Training Program (2023T SYCLJ0028), the National Clinical Key Specialty Construction Project (grant number: Bingcaishe [2023] 16), the Clinical Medical Research Center for Laboratory Medicine of Xinjiang Production and Construction Corps (grant number: Bingkefa [2023] 12), the Science and Technology Research Program in Key Areas of Xinjiang Production and Construction Corps (grant number: 2022AB030 [2022]).

References

1 X. L. Xu, S. W. Ge, C. N. Chen, M. Wen, J. Y. Fu and J. Mod, *Lab. Med.*, 2021, **36**, 140–143.
2 J. Y. Zeng, *Selection and Characterization of DNA Aptamers for H1N1, H3N2 and influenza B virus*, Huaqiao University, 2021, DOI: 10.27155/d.cnki.ghqiu.2021.000644.
3 L. Jennings, Q. S. Huang, L. Barr, P. Lee, W. J. Kim, P. Buchy, M. Sannicas, B. A. Mungall and J. Chen, *Influenza Other Respir. Viruses*, 2018, **12**, 383–411.
4 H. Zaraket, A. C. Hurt, B. Clinch, L. Barr and N. Lee, *Antiviral Res.*, 2021, **185**, 104970.
5 Y. Chen, Q. Liu and D. Guo, *J. Med. Virol.*, 2020, **92**, 418–423.
6 S. Leopardi, E. C. Holmes, M. Gastaldelli, L. Tassoni, P. Priori, D. Scaravelli, G. Zamperin and P. D. Benedictis, *Infect., Genet. Evol.*, 2018, **58**, 279–289.
7 L. Bai, Y. L. Zhao, J. Z. Dong, S. Liang, M. Guo, X. J. Liu, W. Xin, Z. X. Huang, X. Y. Sun, Z. Zhang, L. H. Dong, Q. Y. Liu, Y. C. Zheng, D. P. Niu, M. Xiang, K. Song, J. J. Ye, W. C. Zheng, Z. D. Tang, M. L. Tang, Y. Zhou, C. Shen, M. Dai, L. Zhou, Y. Chen, H. Yan, K. Lan and K. Xu, *Cell Res.*, 2021, **31**, 395–403.
8 S. V. Vemula, J. Q. Zhao, J. K. Liu, X. Wang, S. Biswas and I. Hewlett, *Viruses*, 2016, **8**, 96.
9 S. H. Zhang, H. Tian, N. Jiang, X. C. Wang, H. Huang, C. C. Li, X. X. Kong, C. Dong, L. Zhou, J. F. Peng, X. L. Guo, H. Jin and L. G. Zhu, *J. Southeast Univ.*, 2023, **42**, 439–445.
10 X. G. Wang, G. Lu, J. J. Cheng, S. Q. Cheng, L. T. Zhong, Z. Y. Lai, B. Jia, L. Xu, J. J. Ou, Y. Q. Xiao, X. R. Hu, F. Wang, M. T. Lai, R. Shao, F. Y. Zheng and L. G. Yuan, *Heilongjiang Anim. Sci. Vet. Med.*, 2023, 83–89.
11 J. D. Zhao, Y. H. Li, R. R. Li, V. Timira, B. P. Dasanayaka, Z. Y. Zhang, J. K. Zhang, H. Lin and Z. X. Li, *Food Control*, 2022, **138**, 108983.
12 X. Li, *Respiratory disease isothermal nucleic acid detection system based on microfluidic technology*, University of Chinese Academy of Sciences, 2023, DOI: 10.27522/d.cnki.gkcgs.2023.000201.
13 Z. W. Zhang, P. Ma, R. Ahmed, J. Wang, D. Akin, F. Soto, B. F. Liu, P. W. Li and U. Demirci, *Adv. Mater.*, 2021, **34**, 2103646.
14 M. Park, J. W, B. Y. Choi and C. J. Lee, *Exp. Mol. Med.*, 2020, **52**, 963–977.
15 Z. Z. Liu, *Study on rapid and highly sensitive quantitative detection technology of respiratory viruses based on magnetic SERS immunochromatography*, Academy of Military Sciences, 2023, DOI: 10.27193/d.cnki.gjsky.2023.000086.
16 P. Brangel, A. Sobarzo, C. Parolo, B. S. Miller, P. D. Howes, S. Gelkop, J. J. Lutwama, J. M. Dye, R. A. Mckendry, L. Lobel and M. M. Stevens, *ACS Nano*, 2018, **12**, 63–73.
17 C. W. Wang, C. G. Wang, X. L. Wang, K. L. Wang, Y. H. Zhu, Z. Rong, W. Y. Wang, R. Xiao and S. Q. Wang, *ACS Appl. Mater. Interfaces*, 2019, **11**, 19495–19505.
18 S. S. Lin, Y. S. Zheng, Y. L. Xing, K. Dou, R. Wang, H. W. Cui, R. Wang and F. B. Yu, *Talanta*, 2024, **280**, 126691.
19 C. N. Wang, G. P. Xu, W. J. Wang, Z. Y. Ren, C. M. Zhang, Y. Gong, M. W. Zhao, Y. Y. Qu, W. F. Li, H. T. Zhou and Y. Q. Li, *Biosens. Bioelectron.*, 2023, **237**, 115497.
20 Y. Sun, L. Xu, F. D. Zhang, Z. G. Song, Y. W. Hu, Y. J. Ji, J. Y. Shen, B. Li, H. Z. Lu and H. F. Yang, *Biosens. Bioelectron.*, 2017, **89**, 906–912.

21 J. Qian, L. L. Zhao, Y. B. Huang, C. X. Zhao, H. Liu, X. R. Liu, Z. Y. Cheng and F. B. Yu, *Chem. Eng. J.*, 2024, **482**, 149012.
22 L. C. Lu, J. L. Yu, X. X. Liu, X. S. Yang, Z. H. Zhou, Q. Jin, R. Xiao and C. W. Wang, *RSC Adv.*, 2020, **10**, 271–281.
23 J. F. Wang, X. Z. Wu, C. W. Wang, Z. Rong, H. M. Ding, H. Li, S. H. Li, N. S. Shao, P. T. Dong, R. Xiao and S. Q. Wang, *ACS Appl. Mater. Interfaces*, 2016, **8**, 19958–19967.
24 X. F. Jia, C. W. Wang, Z. Rong, J. Li, K. L. Wang, Z. W. Qie, R. Xiao and S. Q. Wang, *RSC Adv.*, 2018, **8**, 21243–21251.
25 L. Russo, M. S. Purrà, C. R. Quijada, B. M. Leonardo, V. Puntes and K. H. Schifferli, *Nanoscale*, 2019, **11**, 10819–10827.
26 Z. Z. Liu, C. W. Wang, S. Zheng, X. S. Yang, H. Han, Y. W. Dai and R. Xiao, *Nanomedicine*, 2023, **47**, 102624.
27 X. X. Liu, X. S. Yang, K. Li, H. F. Liu, R. Xiao, W. Y. Wang, C. W. Wang and S. Q. Wang, *Sens. Actuators, B*, 2020, **320**, 128350.
28 Y. Li, X. J. Liu, J. C. Guo, Y. T. Zhang, J. H. Guo, X. G. Wu, B. Wang and X. Ma, *Nanomaterials*, 2021, **11**, 1496.
29 M. S. Purrà, B. R. Solvas, C. R. Quijada, B. M. Leonardo and K. H. Schifferli, *ACS Infect. Dis.*, 2017, **3**, 767–776.
30 D. Zhang, L. Huang, B. Liu, E. Su, H. Y. Chen, Z. Z. Gu and X. W. Zhao, *Sens. Actuators, B*, 2018, **277**, 502–509.
31 F. Di. Nardo, E. Alladio, C. Baggiani, S. Cavalera, C. Giovannoli, G. Spano and L. Anfossi, *Talanta*, 2019, **192**, 288–294.
32 Y. Mao, Y. Sun, J. Xue, W. B. Lu and X. W. Cao, *Anal. Chim. Acat.*, 2021, **1178**, 338800.
33 Q. Bayin, L. Huang, C. H. Ren, Y. S. Fu, X. Ma and J. H. Guo, *Talanta*, 2021, **227**, 122207.
34 R. P. Chen, H. Wang, C. Q. Sun, Y. G. Zhao, Y. He, M. S. Nisar, W. S. Wei, H. Q. Kang, X. L. Xie, C. M. Du, Q. Y. Luo, L. Yang, X. F. Tang and B. H. Xiong, *Talanta*, 2023, **258**, 124401.
35 H. F. Liu, E. Dai, R. Xiao, Z. H. Zhou, M. L. Zhang, Z. K. Bai, Y. Shao, K. Z. Qi, J. Tu, C. W. Wang and S. Q. Wang, *Sens. Actuators, B*, 2021, **329**, 129196.